Supplement of Atmos. Chem. Phys., 20, 13929–13955, 2020
https://doi.org/10.5194/acp-20-13929-2020-supplement
© Author(s) 2020. This work is distributed under
the Creative Commons Attribution 4.0 License.

Atmospheric Chemistry and Physics
Open Access

Supplement of

Baffin Bay sea ice extent and synoptic moisture transport drive water vapor isotope (δ^{18}O, δ^{2}H, and deuterium excess) variability in coastal northwest Greenland

Pete D. Akers et al.

Correspondence to: Pete D. Akers (pete.d.akers@gmail.com)

The copyright of individual parts of the supplement might differ from the CC BY 4.0 License.

S1 Quality checking and instrument stability issues

The raw data from the L2130-i was passed through a series of quality checks prior to humidity response correction to remove readings that were well outside typical values observed at Thule. Most of these erroneous readings appear due to liquid water contamination of the intake tubing, likely from precipitation during intense cyclones. These quality checks identified and removed data where:

- L2130-i diagnostic data (e.g., chamber temperature, pressure, status, etc.) were unstable or out of typical ranges
- Water vapor mixing ratio >15000 ppmv
- $\delta^{18}O$ values >-15‰ AND *dxs* values <-20‰
- Standard deviation for five minute aggregates of $\delta^{18}O$ >8‰

An additional quality check was performed after humidity response calibration. Visual inspection was used to identify clearly abnormal isotopic or mixing ratio values (e.g., very large and/or abrupt changes not supported by meteorological data), and these observations were removed.

The machine was initially used at a tundra-based field site in Thule for a summer project in 2015, and it was installed its present location in October 2016. However, there were issues with cavity pressure stability and irregular isotopic readings which culminated in a full systems crash in May 2017. The system was restored on 04 Aug 2017 with stable cavity pressure that has continued through present. Data from before the system restoration has poor correlation in water vapor mixing ratio between the L2130-i and the SMT weather station. Winter isotopic values and mixing ratios are also much higher in the pre-restoration data than the next two winters despite generally similar winter weather. Out of caution, we have restricted our analyses and discussion to only post-restoration data.

S2 Humidity response calibrations

To correct for $\delta^{18}O$ and $\delta^{2}H$ accuracy and precision bias at low water vapor mixing ratios, we injected standard waters for ten minutes at ten different flow rates. The last 200 observations of each injection were saved, and a nonlinear regression was performed on the δX vs. mixing ratio relationship, where δX is either $\delta^{18}O$ or $\delta^{2}H$, to determine accuracy corrections. The nonlinear regression was of the form:

$$\delta X_{correction} = a + \frac{b}{q} \tag{S1}$$

where $\delta X_{correction}$ is the difference between the observed isotopic value and the actual standard isotopic value, q is the water vapor mixing ratio, and a and b are constants. Calculated values for regression parameters are given in Table S4. Confidence intervals for predicted humidity response corrections were estimated using the predictNLS function from the *propagate* package in R.

Changes in analytical precision at low water vapor mixing ratios were calculated with a nonlinear regression of the form:

$$\delta X_{precision} = a + \frac{b}{q} \quad \text{(S2)}$$

where $\delta X_{precision}$ is the standard error of the mean isotopic value for a given flow rate, q is the water vapor mixing ratio, and a and b are constants. Calculated values for regression parameters are given in Table S5.

S3 Isotope–isotope relationships

Over the full dataset, $\delta^{18}O$ and $\delta^{2}H$ have a strong linear relationship with low parameter standard error: $\delta^{2}H = 6.959 \pm 0.003 * \delta^{18}O - 18.07 \pm 0.09$‰ ($r^2 = 0.98$, n=111138, 10 min data). Overall, this value is comparable to other slopes observed at other high latitude sites, such as 6.8 at Ivittuut, Greenland, (Bonne et al., 2014), 6.5 at NEEM, Greenland, (Steen-Larsen et al., 2013), 6.0–6.5 at Dome C, Antarctica (Casado et al., 2016), and 6.95 from the vapor mixing line at Kangerlussuaq, Greenland (Kopec et al., 2014). Changes in $\delta^{18}O$ are thus closely mirrored in $\delta^{2}H$, and most differences are only detectable on very short timescales (i.e., less than hourly) when some minor lead-lag between relative maxima and minima may occur. The *dxs* at Thule is negatively correlated with both $\delta^{18}O$ and $\delta^{2}H$ (ρ_{10min} = -0.78 and -0.70, respectively).

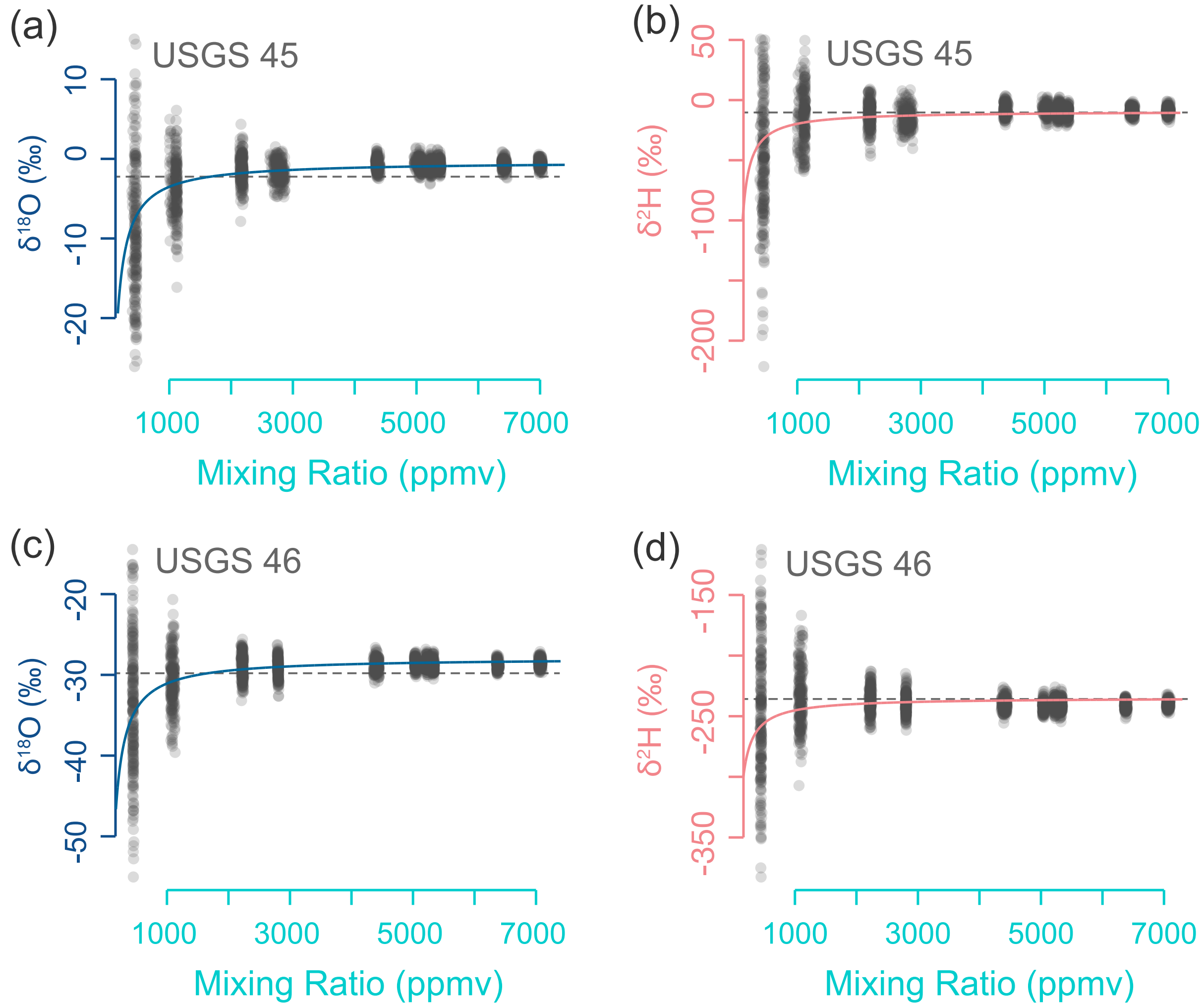

Figure S1. Results of the humidity response calibrations for $\delta^{18}O$ (a, c) and $\delta^{2}H$ (b, d) for two standard waters (USGS 45: top row and USGS 46: bottom row). Points show individual 1 s^{-1} observations, while solid lines show the nonlinear regression of the data (blue: $\delta^{18}O$, pink: $\delta^{2}H$). Dashed horizontal lines show the actual isotopic value of the standard waters.

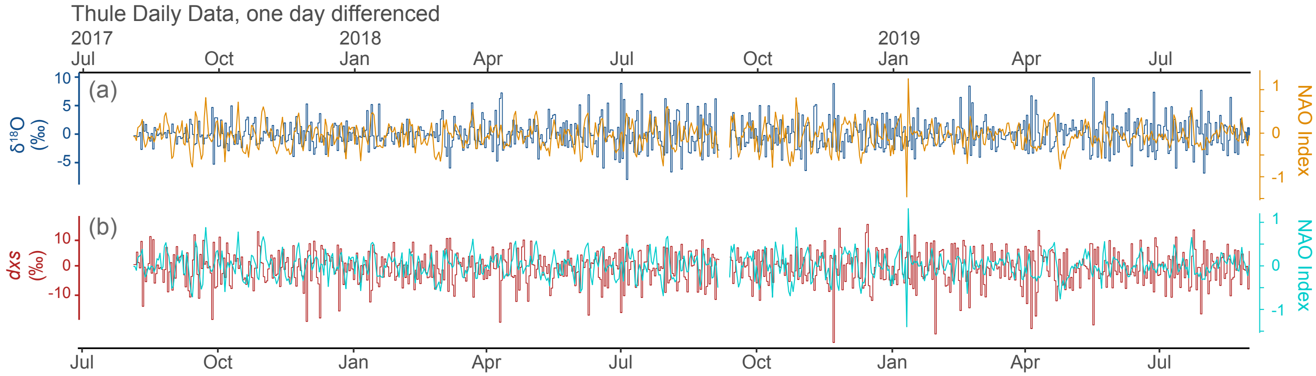

Fig S2: Comparison between time series of (a) $\delta^{18}O$ and (b) *dxs* with NAO index, after all data have been differenced by one day.

50

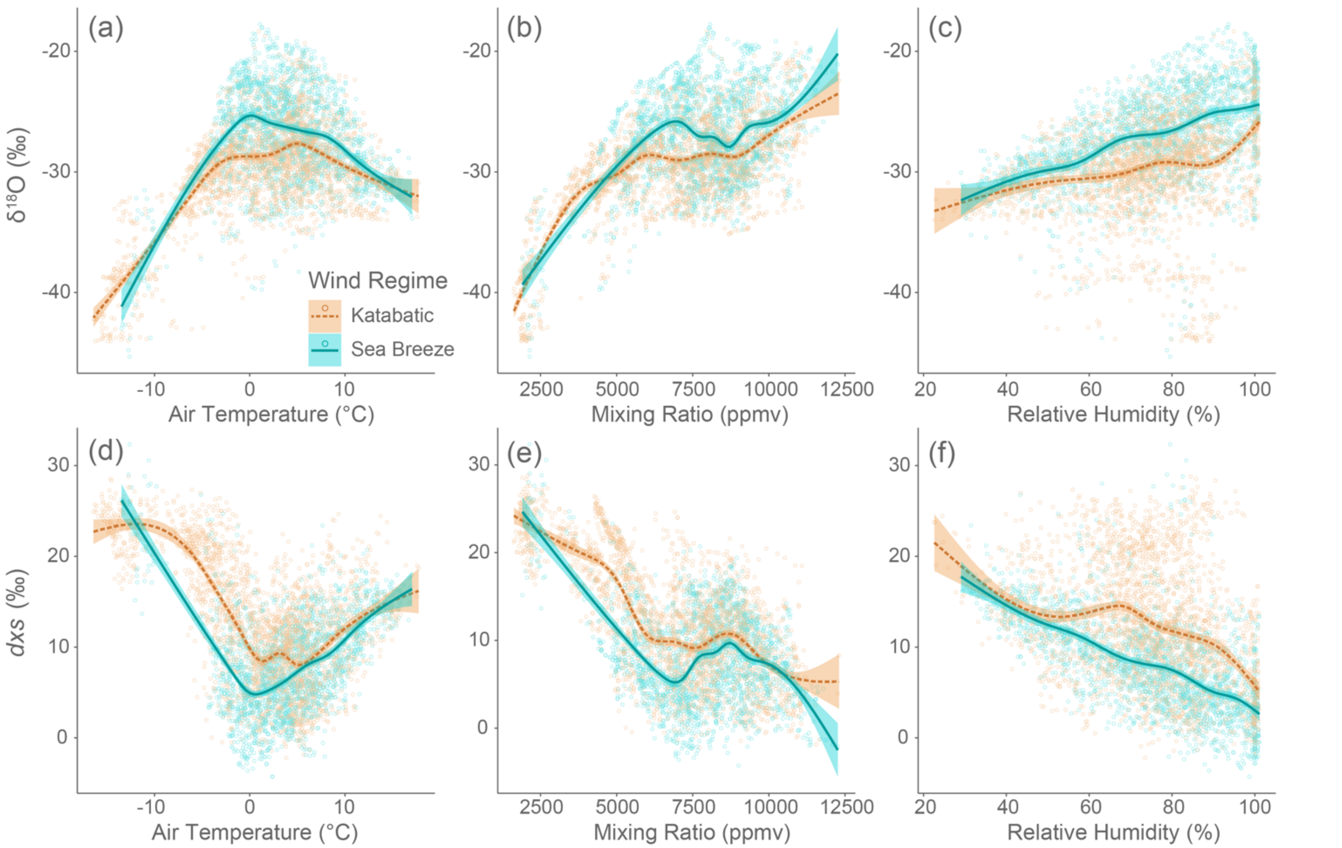

Figure S3. Water vapor $\delta^{18}O$ (top row; a–c) and *dxs* (bottom row; d–f) compared to meteorological variables for the period April through September. Data are split by whether the wind regime was katabatic (azimuth > 40° & < 180°) or sea breeze (azimuth > 240° & < 360°). A generalized additive smoothing model with 95% confidence intervals is overlaid to show trends of the mean values for each wind regime.

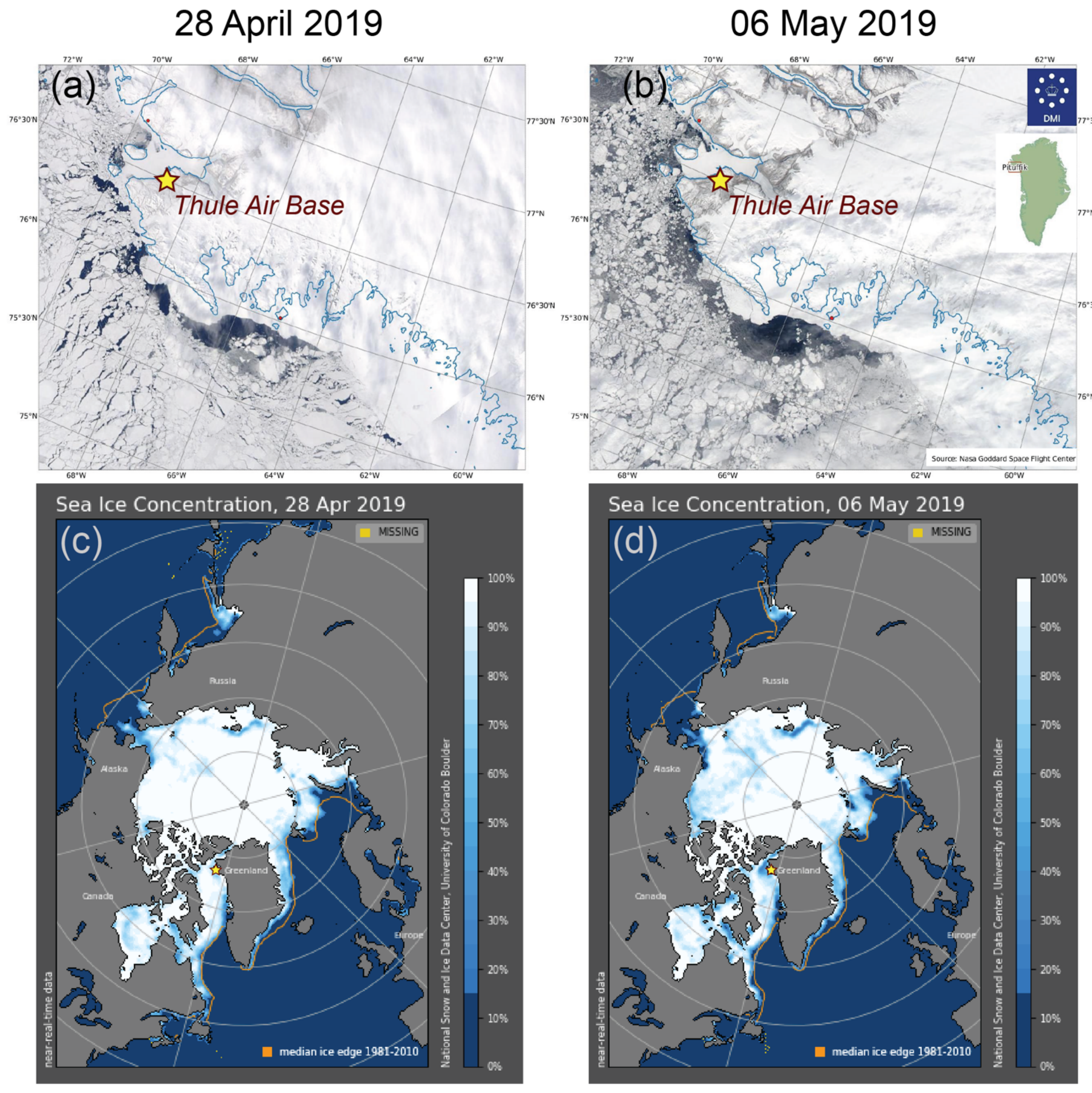

Figure S4: Satellite imagery (top row; a, b) and sea ice concentration (bottom row; c, d) illustrating sea ice conditions before (left column; a, c) and after (right column; b, d) the late spring shift in isotopic and meteorological values at Thule in 2019. The images illustrate the opening of local oceans and snowpack melt as a result of local sea ice breakup. Satellite imagery provided by MODIS (Hall and Riggs, 2015) and sea ice concentration by the NSIDC (Fetterer et al., 2017).

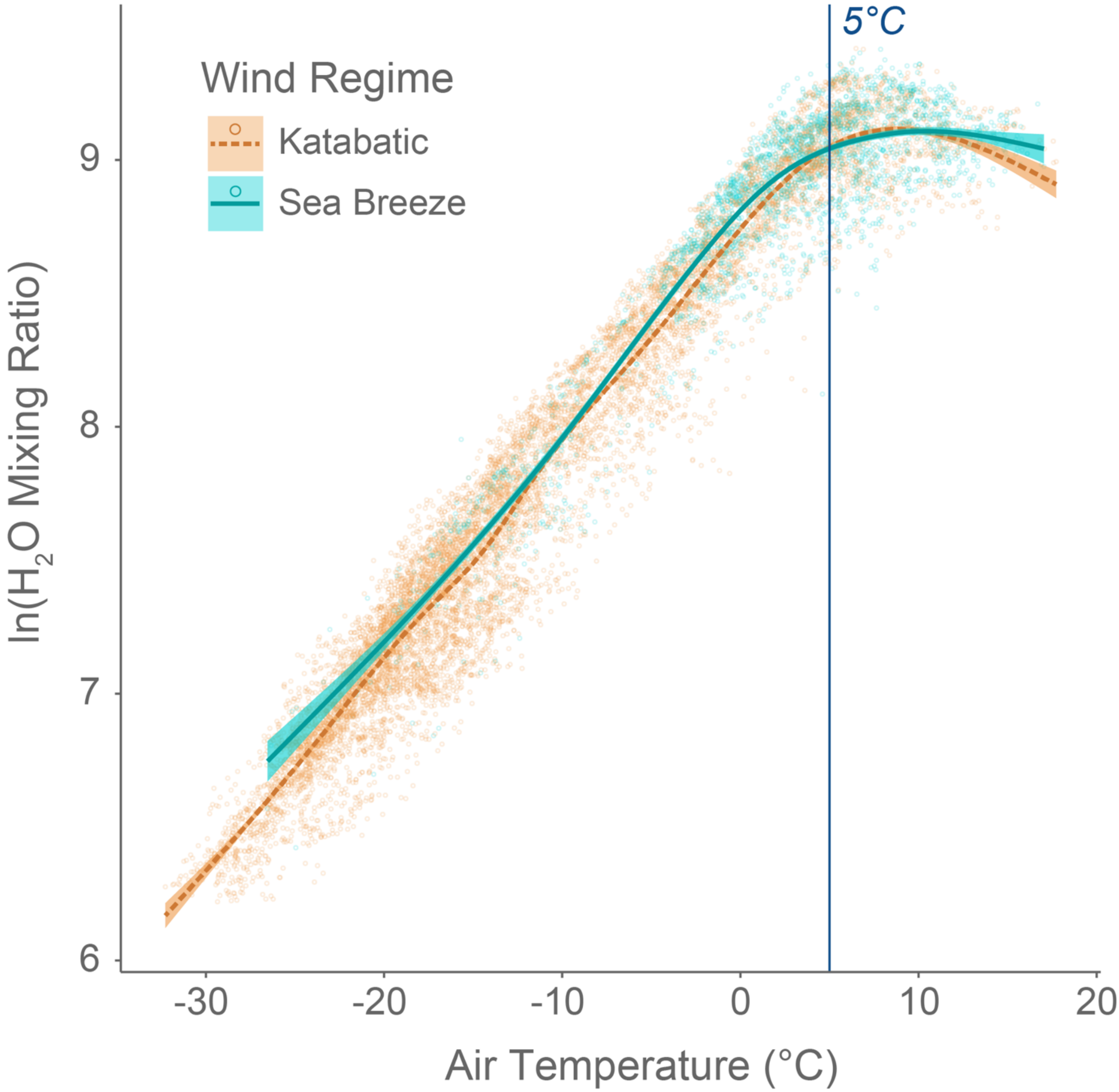

Figure S5. Relationship between air temperature and water vapor mixing ratio (here, log-transformed), illustrating the decoupling that occurs above 5°C (vertical line). Data are split by whether the wind regime was katabatic (azimuth > 40° & < 180°) or sea breeze (azimuth > 240° & < 360°). A generalized additive smoothing model with 95% confidence intervals is overlaid to show trends of the mean values for each wind regime. The relationship decoupling exists in the data from both wind regimes.

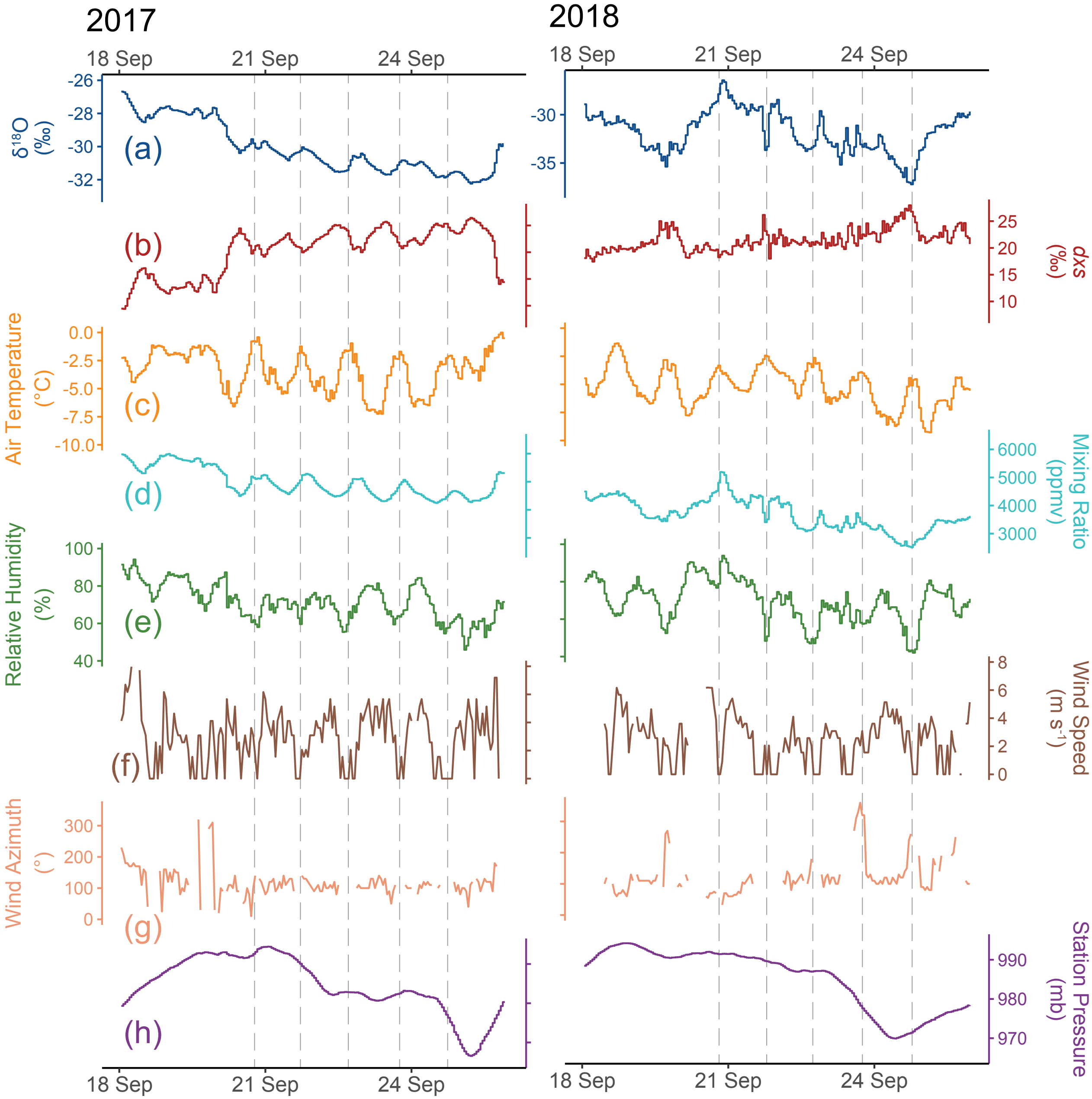

Figure S6. Comparison of isotopic and meteorological data during the period 18–26 Sep for 2017 (left) and 2018 (right). A diel cycle is observed in air temperature, relative humidity, and wind speed in both years, but in the isotopes and mixing ratio only for the year 2017. Y-axes are scaled the same for both years with the exception of δ^{18}O. Dashed gray vertical lines indicate the time of daily thermal max from 20–25 Sep. The 2018 example, when no little to no isotopic cycling is observed, is representative of nearly all other autumn periods at Thule when diel cycles in temperature and relative humidity can be clearly observed in the general time series data.

Table S1. High latitude stationary sites with continuous observations of water vapor isotopes longer than two weeks reported in scientific literature.

Site	Coordinates	Elevation	Setting	Period of record	Citation
Thule, NW Greenland	76.51°N, 68.74°W	229 m a.s.l.	Coastal	08/2017 to 08/2019	This study
Ivittuut, S Greenland	61.21°N, 48.17°W	30 m a.s.l.	Coastal	09/2011 to 05/2013	(Bonne et al., 2014)
Kangerlussuaq, W Greenland	67.02°N, 50.69°W	49 m a.s.l	Coastal	07/2011 to 08/2011	(Kopec et al., 2014)
NEEM, NW Greenland	77.45°N, 51.05°W	2484 m a.s.l.	Ice sheet	05/2010 to 07/2010; 07/2011 to 08/2011; 05/2012 to 08/2012	(Steen-Larsen et al., 2013; Steen-Larsen et al., 2014)
Summit, Greenland	72.58°N, 38.46°W	3216 m a.s.l.	Ice sheet	Summer 2011 to summer 2014	(Bailey et al., 2015)
Selvogsviti, Iceland	63.83°N, 21.47°W	0 m a.s.l.	Coastal	11/2011 to 04/2013	(Steen-Larsen et al., 2015)
Kourovka, W Siberia	57.04°N, 59.55°E	300 m a.s.l.	Inland	09/2012 to 08/2013	(Bastrikov et al., 2014)
Samoylov Island, E Siberia	72.37°N, 126.48°E	0 m a.s.l.	Coastal	07/2015 to 06/2017	(Bonne et al., 2020)
Toolik Lake, N Alaska	68.63°N, 149.60°W	760 m a.s.l.	Inland	05/2013 to 08/2013	(Klein et al., 2015)
Dumont d'Urville, E Antarctica	66.65°S, 140.00°E	10 m a.s.l.	Coastal	12/2016 to 02/2017	(Bréant et al., 2019)
Syowa, E Antarctica	69.00°S, 39.58°E	0 m a.s.l.	Coastal	12/2013 to 02/2014; 12/2014 to 02/2015	(Kurita et al., 2016)
Kohnen, E Antarctica	75.00°S, 0.07°E	2892 m a.s.l	Ice sheet	12/2013 to 01/2014	(Ritter et al., 2016)
Dome C, E Antarctica	75.10°S, 123.39°E	3233 m a.s.l	Ice sheet	12/2014 to 01/2015	(Casado et al., 2016)

Table S2. Standard waters calibration results after dry air system installation, performed roughly every 25 hours. Mean values and standard deviations of the last 200 observations for each calibration are given here. Some days do not have data due to failed calibration from a clogged injection needle or stuck injection piston. Some of the calibrations included here extend beyond the limit of ambient data discussed in the study, but station operation has continued without interruption.

	USGS 45						USGS 46					
	Mixing ratio (ppmv)		$\delta^{18}O$ (‰)		$\delta^{2}H$ (‰)		Mixing ratio (ppmv)		$\delta^{18}O$ (‰)		$\delta^{2}H$ (‰)	
Date	**Mean**	**SD**	**Mean**	**SD**	**Mean**	**SD**	**Mean**	**SD**	**Mean**	**SD**	**Mean**	**SD**
2019-08-01	5367	20	-0.8	0.6	-11	4	5325	14	-28.8	0.6	-241	4
2019-08-02	5378	16	-0.9	0.6	-9	4	5345	10	-28.9	0.6	-239	4
2019-08-04	5412	19	-0.7	0.7	-10	4	5396	14	-28.7	0.6	-240	4
2019-08-05	5421	18	-0.8	0.6	-10	4	5406	14	-28.8	0.6	-241	4
2019-08-06	5450	15	-0.7	0.6	-10	4	5446	17	-28.7	0.6	-240	4
2019-08-07	5459	15	-0.6	0.6	-10	4	5430	18	-28.6	0.6	-240	4
2019-08-09	5480	16	-0.7	0.6	-10	4	5431	17	-28.8	0.6	-240	4
2019-08-10	5438	12	-0.9	0.6	-10	4	5448	19	-28.7	0.6	-239	4
2019-08-11	5467	15	-0.8	0.6	-10	4	5476	59	-28.5	0.6	-239	4
2019-08-12	5392	57	-0.8	0.7	-10	4	5531	91	-28.5	0.7	-240	4

2019-08-14	5520	20	-0.7	0.6	-9	4		5524	18	-28.6	0.7	-239	4
2019-08-15	5523	13	-0.8	0.6	-10	4		5528	21	-28.8	0.6	-240	4
2019-08-16	5574	19	-0.6	0.6	-10	4		5568	20	-28.5	0.6	-240	4
2019-08-17	5599	31	-0.6	0.6	-9	4		5535	38	-28.4	0.6	-239	4
2019-08-18	5492	38	-0.5	0.7	-9	4		5545	24	-28.8	0.7	-240	4
2019-08-19	5478	61	-0.9	0.6	-10	4		5573	20	-28.6	0.6	-239	4
2019-08-20	5610	18	-0.5	0.6	-9	4		5544	79	-28.8	0.6	-240	4
2019-08-22	5488	43	-1.1	0.6	-11	4		5564	15	-28.6	0.6	-240	4
2019-08-23	5605	13	-0.6	0.6	-9	4		5622	18	-28.6	0.6	-240	4
2019-08-24	5566	17	-0.9	0.6	-10	4		5591	17	-28.6	0.6	-240	4
2019-08-25	5642	9	-0.5	0.5	-10	4		5602	38	-28.3	0.7	-239	4
2019-08-26	5519	32	-1.0	0.6	-11	4		5641	19	-28.6	0.6	-240	4
2019-08-27	5674	18	-0.5	0.6	-9	4		5620	24	-28.6	0.6	-240	4
2019-08-28	5616	14	-0.5	0.6	-10	4		5602	64	-28.8	0.6	-241	4
2019-08-29	5642	13	-0.5	0.6	-9	4		5449	104	-29.1	0.7	-241	4
2019-08-31	5632	11	0.0	0.7	-9	4		5655	18	-28.7	0.7	-241	4
2019-09-01	5719	14	-0.6	0.7	-10	4		5668	17	-28.8	0.6	-240	4
2019-09-02	5727	29	-0.7	0.6	-10	4		5739	15	-28.6	0.6	-240	4
2019-09-03	5628	25	-0.5	0.7	-9	4		5671	20	-28.5	0.6	-241	4
2019-09-05	5687	27	-0.7	0.6	-10	4		5744	18	-28.5	0.6	-240	4
2019-09-06	5787	17	-0.5	0.6	-10	4		5734	21	-28.6	0.6	-241	4
2019-09-08	5769	15	-0.2	0.7	-9	4		5798	21	-28.6	0.6	-240	4
2019-09-09	5739	23	-0.3	0.7	-9	4		5762	20	-28.4	0.6	-241	4
2019-09-10	5729	13	-0.5	0.6	-9	4		5714	43	-28.6	0.6	-240	4
2019-09-11	5810	9	-0.5	0.6	-9	4		5749	19	-28.5	0.6	-240	4
2019-09-12	5737	20	-0.4	0.7	-9	4		5787	57	-28.4	0.6	-240	4
2019-09-13	5793	29	-0.9	0.6	-10	4		5788	28	-28.1	0.6	-239	4
2019-09-14	5871	17	-0.1	0.7	-8	4		5837	27	-28.4	0.6	-240	4
2019-09-16	5689	12	-0.6	0.6	-10	4		5852	24	-28.5	0.6	-240	4
2019-09-17	5723	37	-0.8	0.7	-10	4		5817	21	-28.3	0.7	-239	4
2019-09-18	5855	20	-0.3	0.6	-9	3		5901	35	-28.4	0.6	-240	4
2019-09-19	5864	11	-0.5	0.6	-9	4		5811	30	-28.7	0.7	-241	4
2019-09-20	5948	10	-0.5	0.6	-10	4		5966	14	-28.7	0.6	-241	4
2019-09-22	5942	12	-0.5	0.6	-9	4		5938	11	-28.6	0.6	-241	4
2019-09-24	5999	35	-0.4	0.6	-9	4		6009	17	-28.5	0.6	-240	4

2019-09-25	5933	7	-0.4	0.6	-9	4		5929	15	-28.6	0.6	-240	4
2019-09-26	5887	15	-0.6	0.7	-9	4		5967	18	-28.4	0.6	-239	4
2019-09-27	5792	17	-0.9	0.6	-9	4		5855	21	-29.2	0.7	-242	4
2019-09-28	5887	13	-0.4	0.6	-9	4		5880	13	-28.5	0.6	-240	4
2019-09-29	5832	21	-0.3	0.5	-10	4		5866	16	-28.7	0.6	-241	4
2019-09-30	5815	32	0.1	0.6	-8	4		5837	19	-28.5	0.6	-241	4

Table S3. Isotopic value trends for standard water calibrations performed after dry air system installation (Table S3). Trends are calculated as the slope of the last 200 observations taken during a calibration versus time, with one observation per second. The mean and standard deviation of all calibration runs is given at the bottom of the table.

	USGS 45		USGS 46	
Date	**$\delta^{18}O$ (‰ s^{-1})**	**$\delta^{2}H$ (‰ s^{-1})**	**$\delta^{18}O$ (‰ s^{-1})**	**$\delta^{2}H$ (‰ s^{-1})**
2019-08-01	0.0000	0.0047	0.0006	-0.0043
2019-08-02	0.0004	0.0098	0.0001	0.0056
2019-08-04	0.0019	0.0036	0.0001	-0.0064
2019-08-05	0.0021	0.0008	0.0021	0.0037
2019-08-06	0.0015	-0.0063	0.0011	0.0089
2019-08-07	0.0008	-0.0014	0.0009	0.0004
2019-08-09	0.0014	0.0089	-0.0006	-0.0015
2019-08-10	0.0014	0.0016	0.0001	0.0018
2019-08-11	-0.0002	0.0033	0.0004	0.0061
2019-08-12	-0.0032	0.0059	-0.0003	-0.0030
2019-08-14	0.0013	0.0055	-0.0001	-0.0027
2019-08-15	-0.0001	-0.0106	0.0030	0.0096
2019-08-16	0.0006	0.0052	0.0050	0.0064
2019-08-17	0.0007	0.0038	0.0015	-0.0016
2019-08-18	0.0028	0.0040	0.0039	0.0110
2019-08-19	0.0018	0.0122	0.0012	0.0085
2019-08-20	0.0001	0.0112	0.0008	0.0045
2019-08-22	0.0011	0.0115	0.0019	-0.0067
2019-08-23	-0.0014	0.0010	0.0014	0.0042
2019-08-24	-0.0005	0.0079	0.0002	-0.0020
2019-08-25	-0.0002	0.0122	0.0049	0.0058

2019-08-26	-0.0023	0.0001	-0.0002	0.0041
2019-08-27	0.0015	0.0033	0.0010	0.0060
2019-08-28	-0.0009	0.0078	-0.0023	-0.0082
2019-08-29	-0.0003	0.0017	0.0009	-0.0018
2019-08-31	-0.0026	-0.0083	0.0035	0.0009
2019-09-01	-0.0031	0.0004	0.0017	0.0037
2019-09-02	0.0009	0.0113	0.0022	-0.0043
2019-09-03	0.0011	-0.0011	0.0006	0.0021
2019-09-05	-0.0011	0.0021	0.0026	0.0085
2019-09-06	-0.0002	-0.0034	0.0019	0.0014
2019-09-08	-0.0014	0.0030	0.0025	-0.0038
2019-09-09	-0.0014	-0.0119	0.0018	0.0101
2019-09-10	0.0002	-0.0063	0.0018	-0.0027
2019-09-11	-0.0017	-0.0009	0.0034	0.0017
2019-09-12	-0.0013	0.0051	0.0005	0.0064
2019-09-13	-0.0021	-0.0136	0.0022	0.0015
2019-09-14	-0.0018	0.0093	0.0017	0.0103
2019-09-16	-0.0013	-0.0036	0.0012	0.0079
2019-09-17	-0.0036	0.0061	0.0046	0.0107
2019-09-18	-0.0014	0.0007	0.0017	0.0033
2019-09-19	-0.0018	-0.0035	0.0066	0.0243
2019-09-20	0.0037	0.0074	-0.0007	-0.0059
2019-09-22	-0.0025	-0.0006	-0.0004	-0.0009
2019-09-24	0.0000	0.0086	0.0015	0.0040
2019-09-25	0.0012	0.0037	0.0013	0.0059
2019-09-26	-0.0023	-0.0024	0.0030	0.0114
2019-09-27	0.0013	0.0107	-0.0032	-0.0111
2019-09-28	0.0000	0.0014	0.0016	0.0032
2019-09-29	-0.0016	0.0032	0.0018	-0.0081
2019-09-30	-0.0017	0.0058	0.0004	0.0048
Mean	-0.0003	0.0026	0.0014	0.0026

Standard deviation	0.0016	0.0062	0.0018	0.0064

Table S4. Parameters for nonlinear regression of the humidity response accuracy corrections (Equation S1).

Isotopic species	Parameter	Estimate	Standard error	t value	Pr(>|t|)
$\delta^{18}O$	*a*	1.92	0.061	31.6	<0.001
	b	-3190	80	-42.1	<0.001
$\delta^{2}H$	*a*	1.13	0.41	2.8	0.005
	b	-10500	510	-21.0	<0.001

Table S5. Parameters for nonlinear regression of the humidity response precision (Equation S2).

Isotopic species	Parameter	Estimate	Standard error	t value	Pr(>|t|)
$\delta^{18}O$	*a*	-0.003	0.002	-1.4	0.177
	b	260	3	102.2	<0.001
$\delta^{2}H$	*a*	-0.019	0.016	-1.2	0.238
	b	1690	20	85.7	<0.001

Table S6. Percentage of water vapor uptake attributed to Baffin Bay and the Labrador Sea for moisture arriving at Thule, based on back trajectory analysis and split by meteorological season.

Domain	DJF	MAM	JJA	SON
Entire Baffin Bay (Davis to Nares)	35.6	44.4	51.2	47.2
Labrador Sea	13.7	16.3	12.2	11.7
Entire Baffin Bay + Labrador Sea	49.3	60.7	63.4	58.9

References

Bailey, A., Noone, D., Berkelhammer, M., Steen-Larsen, H. C., and Sato, P.: The stability and calibration of water vapor isotope ratio measurements during long-term deployments, Atmos. Meas. Tech., 8, 4521-4538, 10.5194/amt-8-4521-2015, 2015.

Bastrikov, V., Steen-Larsen, H. C., Masson-Delmotte, V., Gribanov, K., Cattani, O., Jouzel, J., and Zakharov, V.: Continuous measurements of atmospheric water vapour isotopes in western Siberia (Kourovka), Atmos. Meas. Tech., 7, 1763-1776, 10.5194/amt-7-1763-2014, 2014.

Bonne, J. L., Masson-Delmotte, V., Cattani, O., Delmotte, M., Risi, C., Sodemann, H., and Steen-Larsen, H. C.: The isotopic composition of water vapour and precipitation in Ivittuut, southern Greenland, Atmos. Chem. Phys., 14, 4419-4439, 10.5194/acp-14-4419-2014, 2014.

Bonne, J. L., Meyer, H., Behrens, M., Boike, J., Kipfstuhl, S., Rabe, B., Schmidt, T., Schönicke, L., Steen-Larsen, H. C., and Werner, M.: Moisture origin as a driver of temporal variabilities of the water vapour isotopic composition in the Lena River Delta, Siberia, Atmos. Chem. Phys., 2020, 1-34, 2020.

Bréant, C., Dos Santos, C. L., Agosta, C., Casado, M., Fourre, E., Goursaud, S., Masson-Delmotte, V., Favier, V., Cattani, O., Prie, F., Golly, B., Orsi, A., Martinerie, P., and Landais, A.: Coastal water vapor isotopic composition driven by katabatic wind variability in summer at Dumont d'Urville, coastal East Antarctica, Earth and Planetary Science Letters, 514, 37-47, 10.1016/j.epsl.2019.03.004, 2019.

Casado, M., Landais, A., Masson-Delmotte, V., Genthon, C., Kerstel, E., Kassi, S., Arnaud, L., Picard, G., Prie, F., Cattani, O., Steen-Larsen, H. C., Vignon, E., and Cermak, P.: Continuous measurements of isotopic composition of water vapour on the East Antarctic Plateau, Atmos. Chem. Phys., 16, 8521-8538, 10.5194/acp-16-8521-2016, 2016.

Fetterer, F., Knowles, K., Meier, W. N., Savoie, M., and Windnagel, A. K.: Sea Ice Index, Version 3. Extent, Concentration, and Concentration Anomalies, NSIDC: National Snow and Ice Data Center, https://doi.org/10.7265/N5K072F8, 2017.

Hall, D. K., and Riggs, G. A.: MODIS/Aqua Sea Ice Extent Daily L3 Global 1km EASE-Grid Day, Version 6, NASA NSIDC Distributed Active Archive Center, https://doi.org/10.5067/MODIS/MYD29P1D.006, 2015.

Klein, E. S., Cherry, J. E., Young, J., Noone, D., Leffler, A. J., and Welker, J. M.: Arctic cyclone water vapor isotopes support past sea ice retreat recorded in Greenland ice, Scientific Reports, 5, 10.1038/srep10295, 2015.

Kopec, B. G., Lauder, A. M., Posmentier, E. S., and Feng, X.: The diel cycle of water vapor in west Greenland, J. Geophys. Res.-Atmos., 119, 9386-9399, 2014.

Kurita, N., Hirasawa, N., Koga, S., Matsushita, J., Steen-Larsen, H. C., Masson-Delmotte, V., and Fujiyoshi, Y.: Influence of large-scale atmospheric circulation on marine air intrusion toward the East Antarctic coast, Geophys. Res. Lett., 43, 9298-9305, 10.1002/2016gl070246, 2016.

Ritter, F., Steen-Larsen, H. C., Werner, M., Masson-Delmotte, V., Orsi, A., Behrens, M., Birnbaum, G., Freitag, J., Risi, C., and Kipfstuhl, S.: Isotopic exchange on the diurnal scale between near-surface snow and lower atmospheric water vapor at Kohnen station, East Antarctica, The Cryosphere, 10, 1647-1663, 2016.

Steen-Larsen, H. C., Johnsen, S. J., Masson-Delmotte, V., Stenni, B., Risi, C., Sodemann, H., Balslev-Clausen, D., Blunier, T., Dahl-Jensen, D., Ellehoj, M. D., Falourd, S., Grindsted, A., Gkinis, V., Jouzel, J., Popp, T., Sheldon, S., Simonsen, S. B., Sjolte, J., Steffensen, J. P., Sperlich, P., Sveinbjornsdottir, A. E., Vinther, B. M., and White, J. W. C.: Continuous monitoring of summer surface water vapor isotopic composition above the Greenland Ice Sheet, Atmos. Chem. Phys., 13, 4815-4828, 10.5194/acp-13-4815-2013, 2013.

Steen-Larsen, H. C., Masson-Delmotte, V., Hirabayashi, M., Winkler, R., Satow, K., Prie, F., Bayou, N., Brun, E., Cuffey, K. M., Dahl-Jensen, D., Dumont, M., Guillevic, M., Kipfstuhl, S., Landais, A., Popp, T., Risi, C., Steffen, K., Stenni, B., and Sveinbjornsdottir, A. E.: What controls the isotopic composition of Greenland surface snow?, Clim. Past, 10, 377-392, 10.5194/cp-10-377-2014, 2014.

Steen-Larsen, H. C., Sveinbjörnsdottir, A. E., Jonsson, T., Ritter, F., Bonne, J.-L., Masson-Delmotte, V., Sodemann, H., Blunier, T., Dahl-Jensen, D., and Vinther, B. M.: Moisture sources and synoptic to seasonal variability of North Atlantic water vapor isotopic composition, J. Geophys. Res.-Atmos., 120, 5757-5774, 10.1002/2015jd023234, 2015.